

Controlling the thermodynamic stability of intermediate phases in a cationic-amphiphile–water system with strongly binding counterions

Santosh Prasad Gupta and V. A. Raghunathan*

Raman Research Institute, C V Raman Avenue, Bangalore 560 080, India

(Received 11 March 2013; revised manuscript received 23 April 2013; published 8 July 2013)

We have studied the influence of two structurally isomeric organic salts, namely, 2-sodium-3-hydroxy naphthoate (SHN) and 1-sodium-2-hydroxy naphthoate (SHN1), on the phase behavior of concentrated aqueous solutions of the cationic surfactant cetylpyridinium chloride (CPC). Partial phase diagrams of the two systems have been constructed using polarizing optical microscopy and x-ray diffraction techniques. A variety of intermediate phases is seen in both systems for a range of salt concentrations. The CPC-SHN-water system exhibits the rhombohedral and tetragonal mesh phases in addition to the random mesh phase, whereas the CPC-SHN1-water system shows only the tetragonal and random mesh phases. The CPC-SHN-water system also exhibits two nematic phases consisting of cylindrical and disk-like micelles at relatively low and high salt concentrations, respectively. These results show that the concentration of the strongly bound counterion provided by the organic salt can be used as a control parameter to tune the stability of different intermediate phases in amphiphile-water systems.

DOI: [10.1103/PhysRevE.88.012503](https://doi.org/10.1103/PhysRevE.88.012503)

PACS number(s): 61.30.St, 64.70.M–, 61.30.Eb, 61.05.C–

I. INTRODUCTION

Amphiphilic molecules self-assemble in water to form micellar aggregates above the critical micellar concentration (CMC) [1]. At much higher amphiphile concentrations (ϕ_s) these solutions exhibit a variety of thermodynamic phases, characterized by varying degrees of translational and orientational order of the micelles [2]. The phase diagrams of single-chain amphiphiles is in general dominated by the hexagonal (H_I) phase, consisting of cylindrical micelles arranged on a two-dimensional (2D) hexagonal lattice, which occurs over a wide range of ϕ_s . At still higher ϕ_s a lamellar (L_α) phase is observed, made up of a periodic stack of planar amphiphile bilayers separated by water. Further increase in ϕ_s results in inverse' structures, where water-filled regions surrounded by the hydrophilic head groups of the amphiphilic molecules are dispersed in the hydrocarbon matrix. These inverse micellar morphologies are referred to as type II, whereas the direct micellar morphologies are called type I.

The generic phase behavior of amphiphile-water systems, outlined above, can be rationalized in terms of a gradual decrease in the spontaneous mean curvature of the micelle-water interface with increasing ϕ_s , from being positive at low values of ϕ_s to being negative for high values of ϕ_s . Many studies indicate that the morphological transformation from cylinders to bilayers does not take place abruptly, but through a sequence of intermediate shapes, giving rise to a sequence of so-called intermediate phases between the hexagonal and the lamellar phases [3]. Nevertheless, the stability of these intermediate phases remains poorly understood, mainly because of the fact that amphiphile aggregates in many of these phases have nonuniform mean and/or Gaussian curvatures.

Intermediate phases are of three kinds—bicontinuous cubic phases, ribbon phases, and mesh phases; all of them can occur as type I and type II. Bicontinuous cubic phases can be easily

identified by the fact that they are optically isotropic, unlike all other phases found at comparable surfactant concentrations, which are birefringent [4]. Type I bicontinuous cubic phases consist of two interpenetrating, topologically identical networks of cylindrical micelles, separated by water. In type II bicontinuous cubic phases two interpenetrating water channels are separated by a surfactant bilayer. Interestingly, the surface separating the two networks into two equal volumes can be described as a triply periodic minimal surface characterized by vanishing mean curvature everywhere on the surface. Three bicontinuous cubic structures have been reported in amphiphile-water systems, belonging to the space groups $Im3m$, $Ia3d$, and $Pn3m$, usually associated with the P, gyroid, and D triply periodic minimal surfaces, respectively. However, a given space group can, in principle, be realized by more than one triply periodic minimal surface [5].

Ribbon phases consist of long micelles with a roughly elliptical cross section, ordered on a 2D rectangular lattice. Two types of structures have been reported, corresponding to the plane groups $cm\bar{m}$ and pgg [6–8].

Mesh phases are made up of 2D mesh-like aggregates, which can also be described as bilayers with a regular array of monodisperse pores. In the ordered mesh phases the mesh-like aggregates lock into a 3D lattice. On the other hand, the random mesh phase consists of a periodic stacking of these aggregates with no long-range positional correlations of the in-plane structure; this phase can also be described as a lamellar phase with in-plane defects that are weakly correlated (L_α^D). All known structures of ordered mesh phases are either rhombohedral (Rh) (space group $R\bar{3}m$) or tetragonal (T) (space group $I4mm$). The former consists of a three-layer stacking of three-coordinated hexagonal mesh, whereas the latter has a two-layer stacking of four-coordinated square mesh.

Most of the studies on mesh phases, reported in the literature, have been carried out on nonionic surfactants, poly(oxyethylene glycol) alkyl ethers (C_nEO_m), where they occur over a rather wide range of compositions [9–17]. The role of the length of the hydrocarbon chain of the surfactant in

*varaghu@rri.res.in

stabilizing different intermediate phases has been well studied in this class of surfactants. Shorter hydrocarbon chains are found to favor the bicontinuous cubic phase, whereas longer ones induce mesh phases [16]. Interestingly, the ordered mesh phase seen in all these systems has a rhombohedral (Rh) structure [13,14,16]. Mesh phases have also been seen in some anionic surfactants [18–21]. A variety of intermediate phases, such as ribbon, ordered mesh, and bicontinuous cubic, has been seen in the sodium dodecyl sulfate (SDS)–water system, albeit over very narrow ranges of composition [18]. The ordered mesh phase seen in this system has tetragonal (T) symmetry. On the other hand, mesh phases have been observed over wide composition ranges in aqueous solutions of some anionic surfactants with stiffer fluorocarbon chains [19–22]. In these systems the structure of the mesh phase is found to depend critically on the type of the counterion. For example, only a random mesh phase (L_{α}^D) is seen in cesium perfluoro-octanoate, whereas its lithium counterpart shows the T mesh phase in addition to the L_{α}^D phase. The Rh mesh phase is seen in tetramethylammonium perfluorodecanoate, but all mesh phases disappear upon increasing the hydrophobicity of the counterion. The above observations suggest that the balance between the aggregate flexibility, determined by the chain length or degree of fluorination, and the interfacial curvature, determined by the head-group size or the nature of the counterion, decides the relative stability of different intermediate phases [3].

Another system exhibiting mesh phases is cationic-amphiphile mixtures, where the Rh and L_{α}^D mesh phases have been observed for slightly differing chain lengths of the two components, indicating again the fine-tuning of the spontaneous curvature necessary to stabilize these phases [23]. Mesh phases have also been reported in some cationic surfactants in the presence of strongly binding counterions provided by organic salts [24–26]. Such counterions are known to adsorb at the micelle-water interface and lead to a reduction in the spontaneous curvature of the aggregates, with cylindrical micelles formed by the pure surfactant transforming into bilayers as the salt-to-surfactant molar ratio (α) approaches 1. Thus the spontaneous mean curvature of the aggregates in these systems can be conveniently controlled by tuning the concentration of the counterions, and mesh phases are observed over an intermediate range of α . Since the lamellar phase with planar bilayers is observed at higher concentrations of these counterions, their influence on the Gaussian curvature seems to be negligible. Interestingly, changes in the structure of the surfactant head group have been found to influence the stability of ordered mesh phases in these systems, with the Rh phase in the cetyltrimethylammonium bromide (CTAB)–3-hydroxy-2-naphthoate (SHN)–water system being replaced by the T phase upon substituting CTAB with cetylpyridinium bromide (CPB) [25,26].

In the present study we investigate the influence of two structurally isomeric organic salts, namely, 2-sodium-3-hydroxy naphthoate (SHN) and 1-sodium-2-hydroxy naphthoate (SHN1), on the phase behavior of the cationic surfactant cetylpyridinium chloride (CPC). For comparison, the effect of 2,3-dihydroxy naphthalene (DHN) on the same surfactant-water system was also studied. Both the CPC-SHN and the CPC-SHN1 systems are found to exhibit a variety of intermediate phases, depending on the salt-to-surfactant molar

ratio, α , and the water content. Both these systems show ribbon and bicontinuous cubic phases at low values of α . At $\alpha = 0.4$ and 0.5, the CPC-SHN system exhibits a transition between the two ordered mesh phases, as a function of both temperature and water content. On the other hand, only the tetragonal mesh phase is observed in the CPC-SHN1 system at similar values of α . At $\alpha \sim 1$ phase diagrams of both systems are dominated by the lamellar phase. Two nematic phases are also observed with SHN, with the one at lower values of α consisting of cylindrical micelles and the one seen at higher values of α being made up of disk-like micelles. In contrast, DHN has a negligible effect on the phase behavior of CPC, and the micelles remain cylindrical up to $\alpha = 0.75$. These results show that strongly binding counterions, provided by the organic salts, can be used to tune the curvature of the micellar interface and stabilize different intermediate phases. These results are important in leading to a better understanding of the relative stability of different intermediate phases in amphiphile-water systems.

II. MATERIALS AND METHODS

CPC, 3-hydroxy-2-naphthoic acid (HNA), 2-hydroxy-1-naphthoic acid (HNA1), 2,3-dihydroxy naphthalene (DHN),

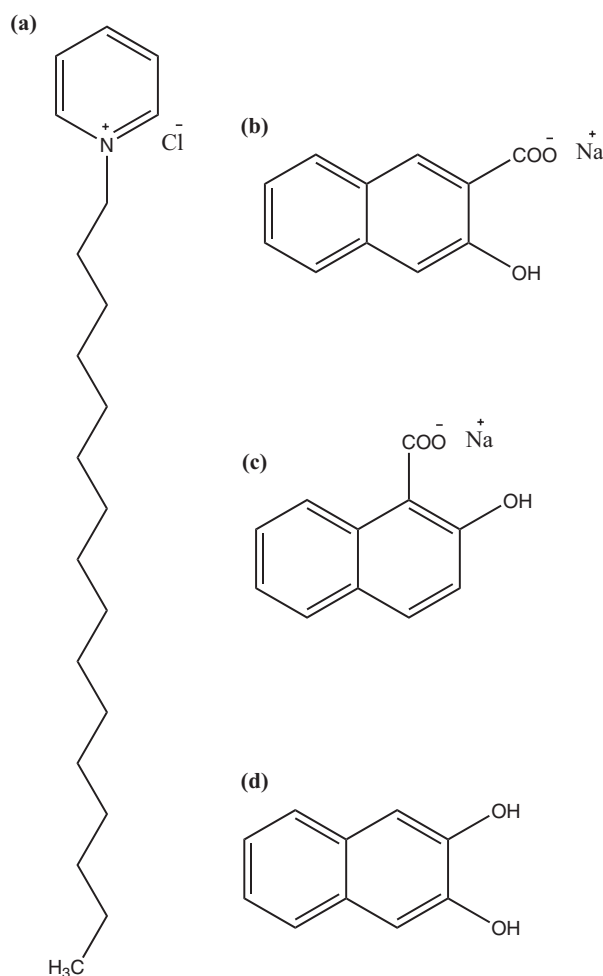


FIG. 1. Chemical structures of (a) cetylpyridinium chloride, (b) 2-sodium-3-hydroxy naphthoate (SHN), (c) 1-sodium-2-hydroxy naphthoate (SHN1), and (d) 2,3-dihydroxy naphthalene (DHN).

and sodium hydroxide (NaOH) were purchased from Sigma-Aldrich. Sodium salts of HNA and HNA1 were prepared by adding an equivalent amount of NaOH to an ethanol solution of the acid [27]. Chemical structures of CPC and the organic salts are shown in Fig. 1. Solutions of appropriate concentration ϕ_s (total wt% of surfactant and organic salt) were prepared by adding deionized water (Millipore) to the surfactant-salt mixture. The sample tubes were then sealed and left in an oven at 40 °C for more than 2 weeks. Samples with different molar ratios ($\alpha = [\text{organic salt}]/[\text{surfactant}]$) were prepared to determine partial phase diagrams of the ternary systems.

Samples were taken between a glass slide and a coverslip for polarizing optical microscopy (POM) observations. Phase transitions were monitored near the center of the sample, far from the edges. For x-ray diffraction studies, samples were taken in 0.5-mm-diameter glass capillaries (Hampton Research) and were flame-sealed. Some of the samples were found to align due to the shear flow at the time of filling the capillaries. Diffraction patterns were obtained using CuK α radiation from a rotating anode x-ray generator (Rigaku UltraX 18) equipped with a collimating multilayer mirror (Xenocs). Data were collected using a 2D image plate detector (Marresearch). Exposures lasted for 20–90 min. Spacings of the sharp peaks in the diffraction pattern could be measured to an accuracy of 0.03 nm, whereas the corresponding quantity for the diffuse peaks was 0.1 nm. Small-angle x-ray scattering studies, covering a range of scattering vector (q) values from

0.01 to 5.0 nm⁻¹, were also carried out using a Hecus S3-Micro system, equipped with a 1D position-sensitive detector (MBraun PSD50M). Typical exposure time was 20 min.

III. RESULTS

A. The CPC-SHN-water system

The phase behavior of these mixtures was studied at $\alpha([\text{SHN}]/[\text{CPC}]) = 0.25, 0.4, 0.5, 0.6, 1.0,$ and 1.25 . For each α , (CPC + SHN) concentration (ϕ_s) was varied from 10 to 80 wt%. Microscopy observations were made over the temperature range from 25 to 85 °C. Phases were identified from their characteristic microscopy textures and diffraction patterns.

At $\alpha = 0.25$ a flow-birefringent isotropic viscoelastic gel (I) is observed at low values of ϕ_s [Fig. 2(a)]. Upon an increase in ϕ_s beyond 30, the samples become birefringent and show POM textures typical of the nematic (N) phase [Fig. 3(a)]. Diffraction patterns of these samples show one broad peak in the small-angle region, confirming the nematic structure [Figs. 4(a) and 5(b)]. Upon a further increase in ϕ_s , the samples exhibit the characteristic texture of the hexagonal (H) phase [Fig. 3(b)]. Diffraction patterns of these samples show two peaks in the small-angle region with their spacings at the ratio $1:1/\sqrt{3}$, consistent with the 2D hexagonal structure [Figs. 4(b) and 5(d)]. The average spacing in the nematic

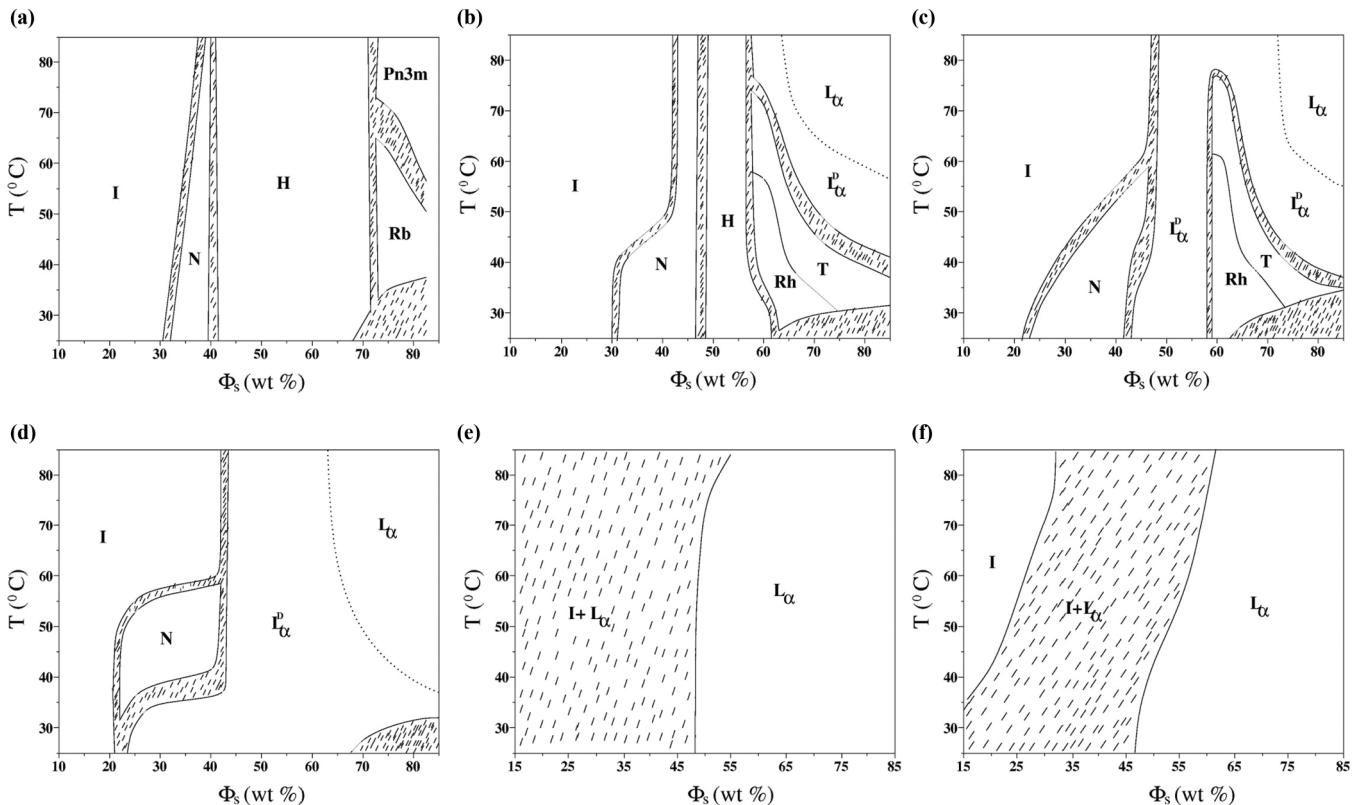


FIG. 2. Partial phase diagram of the CPC-SHN-water system at (a) $\alpha = 0.25$, (b) $\alpha = 0.4$, (c) $\alpha = 0.5$, (d) $\alpha = 0.6$, (e) $\alpha = 1.0$, and (f) $\alpha = 1.25$. *I*, *N*, *H*, *Rb*, *Pn3m*, *Rh*, *T*, L_α^D , and L_α denote the isotropic, nematic, hexagonal, ribbon, bicontinuous cubic, rhombohedral mesh, tetragonal mesh, random mesh, and lamellar phases, respectively. The dotted line indicates the continuous L_α^D - L_α transition. Shaded regions in this and all subsequent phase diagrams correspond to multiphase regions.

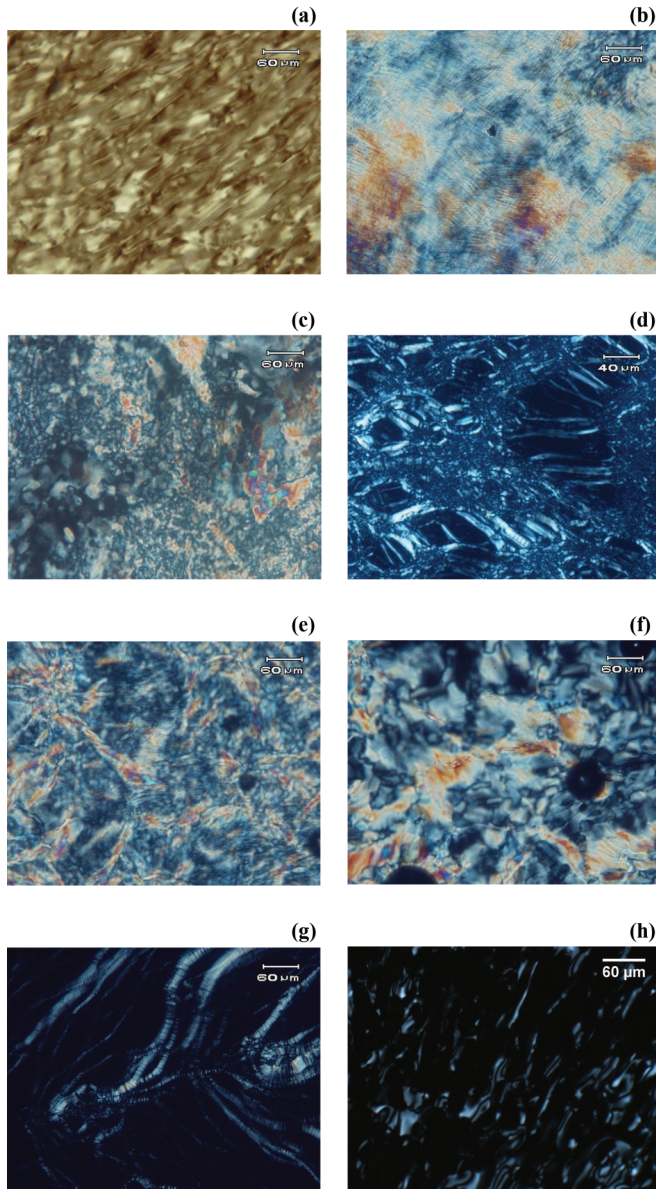


FIG. 3. (Color online) Typical polarizing optical microscopy textures of the (a) N_c , (b) H , (c) R_b , (d) L_α , (e) R_h , (f) T , (g) L_α^D , and (h) N_d phases. The N_c phase is made up of cylindrical micelles, whereas the N_d phase is made up of disk-like micelles.

phase and the lattice parameter of the hexagonal phase decrease with increasing ϕ_s . For $\phi_s > \sim 70$ a crystalline phase coexisting with another birefringent phase is observed at low temperatures. However, upon an increase in temperature a pure phase with a different texture is observed [Fig. 3(c)]. The x-ray diffraction patterns of this phase show five peaks [Fig. 6(b)], which can be indexed on a centered rectangular lattice corresponding to the plane group $cm\bar{m}$ (Table I). We identify this as a ribbon (R_b) phase, which is transformed into an optically isotropic phase upon further increase in the temperature. The x-ray diffraction patterns of the latter phase [Fig. 6(a)] show three peaks with their spacings at the ratio $1/\sqrt{2}:1/\sqrt{3}:1/\sqrt{4}$, and can be indexed on a cubic lattice with space group $Pn\bar{3}m$ (Table II).

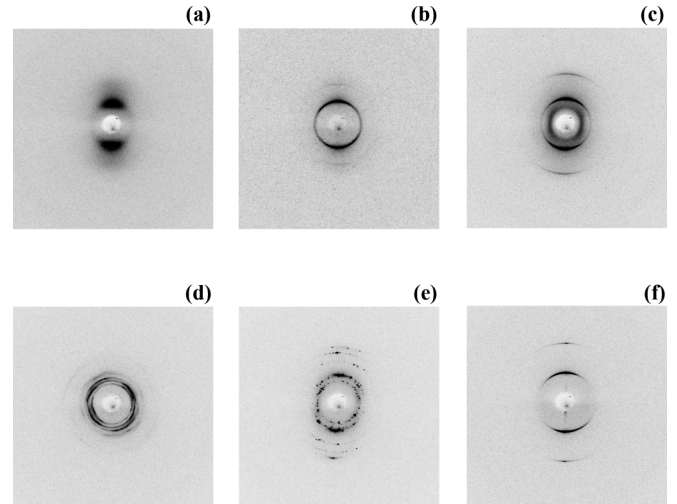


FIG. 4. Partially oriented diffraction patterns of the (a) N_c , (b) H , (c) L_α^D , (d) R_h , (e) T , and (f) L_α phases.

Flow-birefringent isotropic, nematic, and hexagonal phases are also observed at lower values of ϕ_s at $\alpha = 0.4$ [Fig. 2(b)]. However, the concentration range of the H phase is considerably reduced and the phase behavior at higher ϕ_s is very different. A lamellar (L_α) phase is observed in the high- ϕ_s , high-temperature limit. The diffraction patterns of this phase show two peaks with their spacings at the ratio 1:1/2 [Figs. 4(f) and 5(e)]. Three intermediate phases are observed between the H and the L_α phases. Two of these phases (R_h and T) exhibit distinct mosaic POM textures, whereas the third (L_α^D) shows an oily-streak texture similar to the L_α phase [Figs. 3(d)–3(g)]. Diffraction patterns of the R_h phase typically show six peaks [Figs. 4(d) and 6(d)], which can be indexed on a rhombohedral lattice (Table III) with space group $R\bar{3}m$. The T phase also typically shows six peaks in its diffraction pattern [Figs. 4(e) and 6(e)], which can be indexed on a body centered tetragonal

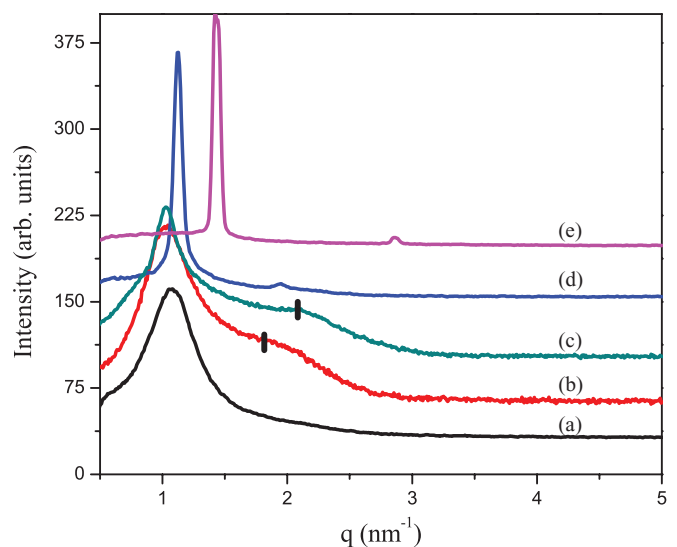


FIG. 5. (Color online) Typical diffraction patterns of the (a) I , (b) N_c , (c) N_d , (d) H , and (e) L_α phases. The bars on curves b and c indicate the secondary peaks at $\sqrt{3}q_0$ and $2q_0$, respectively, where q_0 is the position of the primary peak.

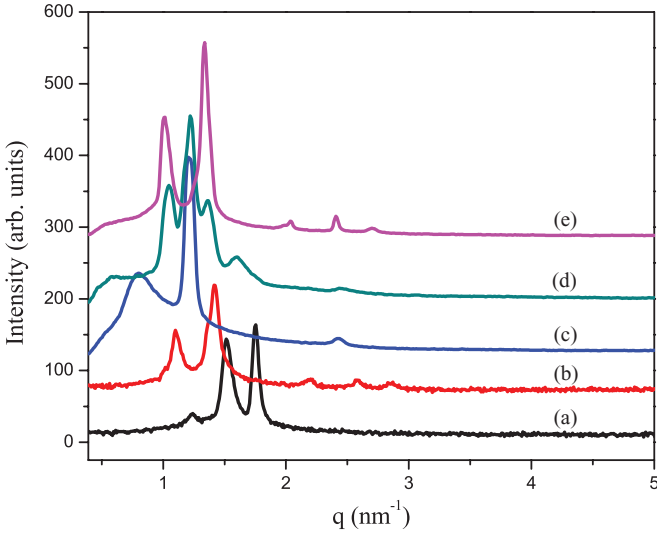


FIG. 6. (Color online) Typical diffraction patterns of the (a) $Pn3m$, (b) Rb, (c) L_α^D , (d) Rh, and (e) T phases of the CPC-SHN-water system.

lattice with space group $I4mm$ (Table IV). Diffraction patterns of the L_α^D phase show a diffuse peak in the small- q region, in addition to two sharp peaks, whose spacings are at the ratio 1:1/2 [Figs. 4(c) and 6(c)]. In oriented samples the diffuse peak appears in the direction normal to the sharp peaks [Fig. 4(c)]. The diffuse peak gradually disappears upon an increase in temperature at high values of ϕ_s and the L_α^D phase transforms continuously into the L_α .

The phase behavior at $\alpha = 0.5$ is very similar to that observed at $\alpha = 0.4$, with the difference that the L_α^D phase is observed at intermediate values of ϕ_s instead of the H phase [Fig. 2(c)]. Further, the nematic phase at this composition shows pseudoisotropic regions in its POM texture, where the optic axis is oriented normal to the glass plates [Fig. 3(h)]. Since rod-like micelles do not exhibit such an orientation, we conclude that this nematic phase is made of disk-like micelles, unlike the one seen at $\alpha = 0.25$ and 0.4, which is made up of long cylindrical micelles. The much lower viscosity of this phase at $\alpha = 0.5$ is in agreement with this conclusion.

At $\alpha = 0.6$ the Rh and T phases seen at $\alpha = 0.5$ disappear and only the I , N , L_α^D , and L_α phases are observed with increasing ϕ_s [Fig. 2(d)]. The phase diagrams at $\alpha = 1.0$ and 1.25 are very similar and dominated by the L_α phase

TABLE I. X-ray diffraction data from the Rb phase of the CPC-SHN-water system at $\alpha = 0.25$, $\phi_s = 80$, and $T = 40$ °C, indexed on a centered rectangular lattice corresponding to the space group cmc . Calculated spacings (d_c) were obtained using the relation $1/d^2 = h^2/a^2 + k^2/b^2$ with the condition $h + k = 2n$, where n is an integer. Unit cell parameters are $a = 7.49$ nm and $b = 8.84$ nm.

d_o (nm)	d_c (nm)	(hk)	Intensity
5.71	5.71	(11)	60
4.42	4.42	(02)	100
2.86	2.86	(22)	10
2.42	2.40	(31)	10
2.21	2.21	(04)	8

TABLE II. X-ray diffraction data from the cubic phase of the CPC-SHN-water system at $\alpha = 0.25$, $\phi_s = 80$, and $T = 60$ °C, indexed on a cubic lattice corresponding to the space group $Pn3m$. Calculated spacings (d_c) were obtained from the relation $1/d^2 = (h^2 + k^2 + l^2)/a^2$, with $a = 7.17$ nm.

d_o (nm)	d_c (nm)	(hkl)	Intensity
5.07	5.07	(110)	20
4.13	4.14	(111)	80
3.59	3.58	(200)	100

[Figs. 2(e) and 2(f)]. It coexists with a low-viscosity isotropic phase at lower values of ϕ_s . A pure isotropic phase is obtained at $\alpha = 1.25$ upon heating.

B. The CPC-SHN1-water system

The phase behavior of these mixtures was studied at $\alpha = 0.25, 0.4, 0.5$, and 1.0. For each α , the (CPC + SHN1) concentration (ϕ_s) was varied from 10 to 80 wt%. Microscopy observations were made over the temperature range from 25 to 85 °C.

The phase behavior of this system at $\alpha = 0.25$ is almost identical to that of the CPC-SHN-water system at the same value of α , except for the fact that the L_α^D phase and an additional cubic phase are observed at high values of ϕ_s at temperatures above the Rb phase [Fig. 7(a)]. Diffraction data from the Rb phase are consistent with the cmc plane group as in the previous case [Table V, Fig. 8(c)]. Diffraction patterns of the higher temperature cubic phase show four peaks, with their spacings at the ratio $1/\sqrt{3}:1/\sqrt{4}:1/\sqrt{11}:1/\sqrt{14}$, and can be indexed on a cubic lattice with the $Pn3m$ space group [Table VI, Fig. 8(b)]. The lower temperature cubic phase shows only two peaks, with their spacings at the ratio $1/\sqrt{6}:1/\sqrt{8}$; we tentatively assign it the space group $Ia3d$ since these spacings correspond to the first two allowed reflections from it, although the other two possible space groups, namely, $Pn3m$ and $Im3m$, are also consistent with the diffraction data [Table VII, Fig. 8(a)].

The phase behavior of this system at $\alpha = 0.4$ is also very similar to that of the previous one, the only difference being that the Rh phase is absent [Fig. 7(b)]. Diffraction data from the T phase is very similar to those obtained from the CPC-SHN system (Table VIII, Fig. 8(e)).

TABLE III. X-ray diffraction data from the Rh phase of the CPC-SHN-water system at $\alpha = 0.40$, $\phi_s = 60$, and $T = 40$ °C, indexed on a rhombohedral ($R\bar{3}m$) lattice. Calculated spacings (d_c) were obtained using the relation $1/d^2 = 4(h^2 + hk + k^2)/3a^2 + l^2/c^2$ with the condition $-h + k + l = 3n$, where n is an integer. Unit cell parameters are $a = 10.77$ nm and $c = 15.28$ nm.

d_o (nm)	d_c (nm)	(hkl)	Intensity
5.91	5.91	(012)	20
5.09	5.09	(003)	100
4.48	4.46	(021)	20
3.72	3.70	(013)	6
2.91	2.90	(015)	3
2.54	2.55	(006)	2

TABLE IV. X-ray diffraction data from the T phase of the CPC-SHN-water system at $\alpha = 0.4$, $\phi_s = 60$, and $T = 65^\circ\text{C}$, indexed on a body centered tetragonal lattice (space group $I4mm$). Calculated spacings (d_c) were obtained using the relation $1/d^2 = (h^2 + k^2)/a^2 + l^2/c^2$ with the condition $h + k + l = 2n$, where n is an integer. Unit cell parameters are $a = 6.69$ nm and $c = 8.69$ nm.

d_o (nm)	d_c (nm)	(hkl)	Intensity
5.30	5.30	(101)	55
4.33	4.35	(002)	100
2.84	2.83	(211)	5
2.38	2.37	(220)	4
2.15	2.17	(004)	3
1.42	1.45	(006)	2

Only the I , L_α^D , and L_α phases are observed at $\alpha = 0.5$ [Fig. 7(c)], and at $\alpha = 1.0$ the L_α^D phase also disappears [Fig. 7(d)]. The I phase at these compositions has a very low viscosity, unlike the one observed at lower values of α . Variation of d in the pure L_α is found to be described by the relation ($d \sim \phi_v^{-s}$) with $s \sim 1$, where ϕ_v is the volume fraction of the nonaqueous component estimated from ϕ_s , using the densities of the components [Fig. 7(f)].

TABLE V. X-ray diffraction data from the ribbon phase of the CPC-SHN1-water system at $\alpha = 0.25$, $\phi_s = 80$, and $T = 42^\circ\text{C}$, indexed on a 2D centered rectangular lattice corresponding to the space group $cm\bar{m}$. Unit cell parameters are $a = 7.25$ nm and $b = 8.60$ nm.

d_o (nm)	d_c (nm)	(hk)	Intensity
5.54	5.54	(11)	10
4.30	4.30	(02)	100
2.34	2.33	(31)	1
2.14	2.15	(04)	1

C. The CPC-DHN-water system

The phase behavior of these mixtures was studied at $\alpha = 0.5$ and 0.75 . For each α , the (CPC + DHN) concentration (ϕ_s) was varied from 10 to 80 wt%. Microscopy observations were made over the temperature range from 25 to 85°C .

The phase behavior of this system is very similar for $\alpha = 0.5$ and $\alpha = 0.75$. At low values of ϕ_s and high temperatures, a viscoelastic isotropic gel is found [Fig. 7(e)]. At higher values of ϕ_s the phase diagram is dominated by the H phase. At much higher values of ϕ_s , DHN crystallizes out of the solution. Figure 7(f) shows the variation of the lattice parameter of the H phase with ϕ_s . It is found to be described by the relation

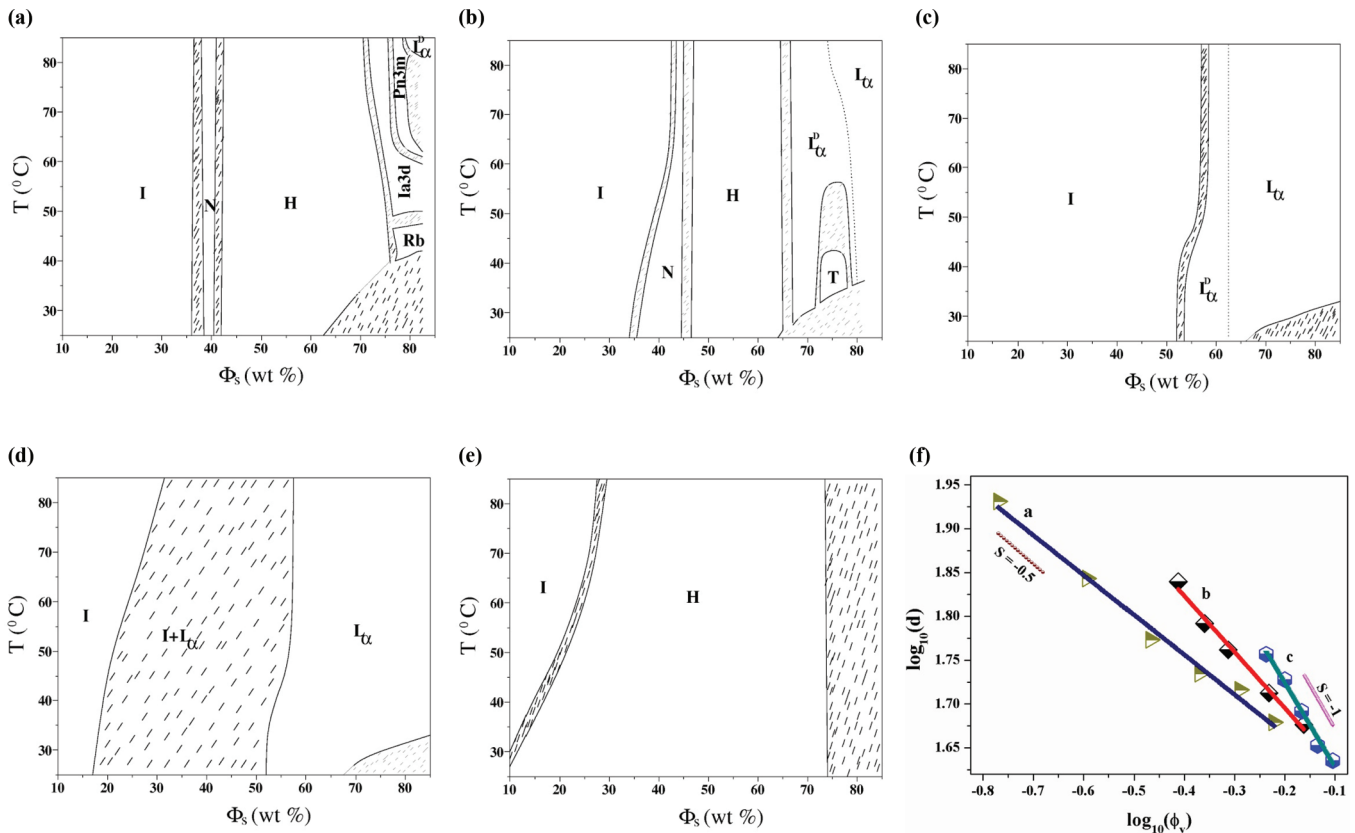


FIG. 7. (Color online) Partial phase diagram of the CPC-SHN1-water system, at (a) $\alpha = 0.25$, (b) $\alpha = 0.4$, (c) $\alpha = 0.5$, and (d) $\alpha = 1.0$. I , N , H , Rb , $Ia3d$, $Pn3m$, L_α^D , T , and L_α denote the isotropic, nematic, hexagonal, ribbon, cubic (Q230), cubic (Q224), random mesh, tetragonal mesh, and lamellar phases, respectively. (e) Partial phase diagram of the CPC-DHN-water system at $\alpha = 0.5$. (f) Variation of the lattice parameters of the H (curve a: CPC-DHN-water, $\alpha = 0.5$, $T = 30^\circ\text{C}$), L_α^D (curve b: CPC-SHN-water, $\alpha = 0.6$, $T = 30^\circ\text{C}$), and L_α (curve c: CPC-SHN1-water, $\alpha = 1.0$, $T = 40^\circ\text{C}$) phases.

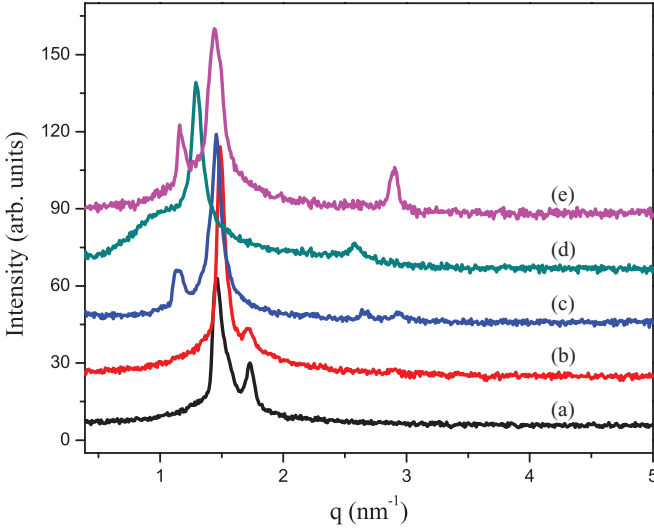


FIG. 8. (Color online) Typical diffraction patterns of the (a) $Ia3d$, (b) $Pn3m$, (c) Rb , (d) L_{α}^D , and (e) T phases of the CPC-SHN1-water system.

($d \sim \phi_v^{-s}$) with $s \sim 0.5$, where ϕ_v is the volume fraction of the nonaqueous component estimated from ϕ_s , using the densities of the components.

IV. DISCUSSION

The high viscosity of the isotropic phase observed at low values of α in all three systems indicates the formation of long worm-like micelles. Such behavior is quite common in ionic surfactants upon the addition of simple inorganic as well as organic salts [28] and is very similar to that seen in mixtures of CTAB with salts such as KBr, sodium salicylate, sodium tosylate, and SHN [24,29–31] and in the CPB-SHN-water system [26]. The formation of these long flexible micelles is attributed to the decrease in the spontaneous curvature of the micelles in the presence of salt, which leads to an increase in the end-cap energy of the cylindrical micelles.

The nematic (N_c) phase that occurs in the CPC-SHN-water and CPC-SHN1-water systems at low values of α is made up of worm-like micelles that have a cylindrical shape on average. This conclusion is supported by the following observations. This phase occurs close to the hexagonal phase and is highly viscous. POM textures of this phase do not exhibit any homeotropic regions, where the optic axis is normal to the bounding plates [Fig. 3(a)]. The x-ray diffraction patterns of

TABLE VI. X-ray diffraction data from the cubic phase of the CPC-SHN1-water system at $\alpha = 0.25$, $\phi_s = 77.5$, and $T = 75$ °C, indexed on a 3D cubic lattice corresponding to the space group $Pn3m$. Calculated spacings (d_c) were obtained using the relation $1/d^2 = (h^2 + k^2 + l^2)/a^2$, with $a = 7.17$ nm.

d_o (nm)	d_c (nm)	(hkl)	Intensity
4.15	4.14	(111)	100
3.59	3.58	(200)	9
2.16	2.16	(311)	1
1.92	1.92	(321)	1

TABLE VII. X-ray diffraction data from the cubic phase of the CPC-SHN1-water system at $\alpha = 0.25$, $\phi_s = 75$, and $T = 75$ °C, indexed on a 3D cubic lattice corresponding to the space group $Ia3d$. Calculated spacings (d_c) were obtained from the relation $1/d^2 = (h^2 + k^2 + l^2)/a^2$, with $a = 10.21$ nm.

d_o (nm)	d_c (nm)	(hkl)	Intensity
4.17	4.17	(211)	100
3.60	3.61	(220)	6

this phase show a secondary maximum near $\sqrt{3}q_o$, where q_o is the wave vector of the primary peak, which indicates short-range hexagonal order [Fig. 5(b)]. A further increase in ϕ_s brings the cylindrical micelles closer, forcing them to order on a 2D hexagonal lattice.

In contrast, the nematic (N_d) phase that occurs at higher values of α in the CPC-SHN-water system is made up of micelles that have a disk-like shape on average. This phase has a much lower viscosity in comparison and occurs close to the lamellar phase. POM textures of this phase show homeotropic regions, where the optic axis is normal to the bounding plates [Fig. 3(h)]. The x-ray diffraction patterns of this phase show a secondary maximum near $2q_o$, indicating short-range lamellar order.

It is possible that a biaxial nematic phase might occur in between the above two uniaxial phases, as found, for example, in the potassium laurate–decanol–water system [32]. Another possibility is that an isotropic phase made up of almost-spherical micelles intervenes between the two uniaxial nematic phases, as found in a closely related system [33]. We plan to probe this part of the phase diagram in more detail to settle this issue.

The observation of a lamellar phase over an extended range of ϕ_s near $\alpha = 1.0$ in the CPC-SHN-water and CPC-SHN1-water systems is reminiscent of the behavior of mixtures of cationic and anionic surfactants [34–36]. Although HN^- and $HN1^-$ counterions are much shorter than the CPC molecule, their incorporation in the CPC micelle seems to have a similar effect as that of a much longer anionic surfactant.

The structure of the rhombohedral mesh phase can be described as a periodic stack of 2D networks of rod-like segments, with three rods meeting at each node [25]. Each unit cell of the 3D hexagonal lattice has a three-layer stacking (ABC) of these mesh-like aggregates. On the other hand, in the tetragonal mesh structure four rods meet at each node. These are stacked with a two-layer repeat, with the centers of the squares in one layer placed on top of the nodes in the

TABLE VIII. X-ray diffraction data from the tetragonal mesh phase of the CPC-SHN1-water system at $\alpha = 0.4$, $\phi_s = 75$, and $T = 35$ °C, indexed on a 3D body centered tetragonal (T) lattice corresponding to the space group $I4mm$. Unit cell parameters are $a = 6.90$ nm and $c = 8.64$ nm.

d_o (nm)	d_c (nm)	(hkl)	Intensity
5.39	5.39	(101)	28
4.32	4.32	(002)	100
2.16	2.16	(004)	9

TABLE IX. Values of the micellar radius obtained using Eq. (1) at different compositions at $T = 40^\circ\text{C}$ in the (a) CPC-SHN-water and (b) CPC-SHN1-water systems. d_d is the spacing of the diffuse peak in the L_α^D phase, d the lamellar periodicity, and a and c the lattice parameters of the Rh and T phases. The ratio of the in-plane and out-of-plane periodicities, γ , is defined as d_d/d for the L_α^D phase, $3a/c$ for the Rh phase, and $2a/c$ for the T phase.

α	ϕ_s	ϕ_v	d_d (nm)	d (nm)	a (nm)	c (nm)	r_m (nm)	γ	Phase
(a)									
0.4	65	0.64	—	—	7.49	8.96	2.07	1.67	T
—	70	0.69	—	—	7.49	8.75	2.13	1.71	T
—	80	0.79	—	—	7.28	8.65	2.27	1.68	T
0.5	45	0.44	7.633	5.62	—	—	1.91	1.36	L_α^D
—	50	0.49	7.413	5.42	—	—	1.96	1.37	L_α^D
—	54	0.53	7.393	5.32	—	—	2.03	1.39	L_α^D
—	56	0.55	7.371	5.27	—	—	2.06	1.40	L_α^D
—	60	0.59	—	—	10.18	14.62	2.36	2.09	Rh
—	65	0.64	—	—	8.03	9.22	2.16	1.74	T
—	70	0.69	—	—	6.70	8.41	1.98	1.60	T
—	80	0.79	5.096	4.17	—	—	1.92	1.22	L_α^D
0.6	50	0.48	7.398	5.69	—	—	2.01	1.30	L_α^D
—	60	0.58	7.234	5.28	—	—	2.13	1.37	L_α^D
—	70	0.69	6.561	4.72	—	—	2.10	1.39	L_α^D
(b)									
0.4	70	0.69	6.08	4.84	—	—	2.08	1.26	L_α^D
—	75	0.74	—	—	6.90	8.64	2.13	1.60	T

next [18,19]. Upon dilution, the layers swell apart to form a lamellar structure where long-range positional correlations of the mesh structure are lost; heating also has a similar effect. Hence, the basic structural unit of the random mesh phase (L_α^D) and the ordered mesh phases (Rh and T) can be expected to be the same.

To verify the above structure, the size of the surfactant aggregates can be calculated from the known surfactant volume fraction. The total volume of the rods in each unit cell can be equated to the surfactant volume fraction ϕ_v in the sample, resulting in the relation [12]

$$4(2 - \pi)r_m^3 + 2\pi ar_m^2 - a^2 d \phi_v = 0, \quad (1)$$

whereas r_m is the micellar radius, $d = c/3$ for the Rh phase and $d = c/2$ for the T phase, a and c being the lattice parameters. ϕ_v was estimated from ϕ_s and densities of the constituent components. The above expression can also be used in the case of the L_α^D phase with $a = d_d$, given by the position of the diffuse peak, and the lamellar periodicity d . Values of r_m obtained from the above expression are listed in Table IX. They are found to be comparable to the values of micellar radii of surfactants with the same chain length, reported in the literature [37], lending support to the proposed models of these phases.

Table IX also lists the values of the ratio of the in-plane periodicity to the stacking periodicity, γ , which is defined as d_d/d for the random mesh, $2a/c$ for the T phase, and $3a/c$ for the Rh phase. Variation of γ with ϕ_s at a few fixed values of α and temperature is shown in Fig. 9. Interestingly, the ordered mesh phases are found to occur only above a critical value of $\gamma \sim 1.5$. This behavior can be understood in terms of the spatially modulated part of the interaction potential between the layers (due to the mesh-like structure), which can be expected to decay almost

exponentially with a decay length of the order of the in-plane periodicity [1]. Only when the separation between adjacent mesh-like layers is slightly lower than the mesh size will the interaction potential be strong enough to lock the layers into a 3D ordered phase. These data also show that the reappearance of the L_α^D phase at higher ϕ_s is a consequence of the decreasing in-plane periodicity (pore size), rather than being due to the screening of the interbilayer interactions, as proposed earlier [21]. The observed decrease in pore size with increasing ϕ_s at a low water content is consistent with earlier

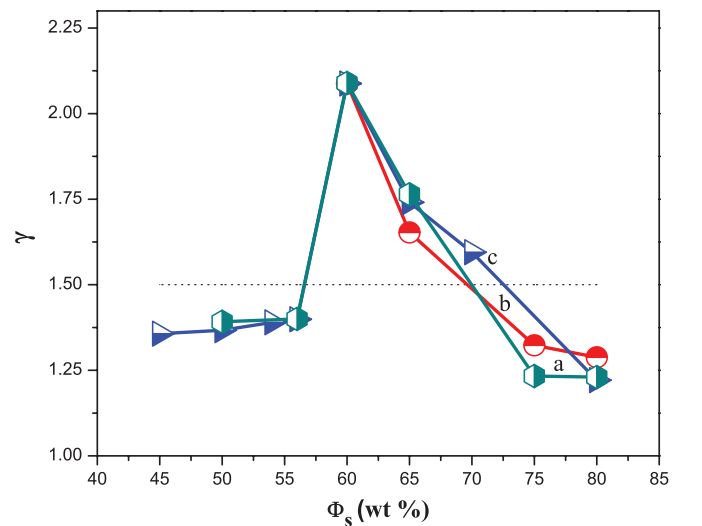


FIG. 9. (Color online) Variation of γ with composition in the CPC-SHN-water system. Curve a: $\alpha = 0.5$, $T = 50^\circ\text{C}$. Curve b: $\alpha = 0.4$, $T = 50^\circ\text{C}$. Curve c: $\alpha = 0.5$, $T = 40^\circ\text{C}$. The dotted line indicates the boundary between the ordered and the random mesh phases.

reports of the annealing of bilayer pores with increasing salt concentration [20].

Figure 7(f) shows the swelling behavior of the L_α^D phase in the CPC-SHN-water system. It is found to be described by the relation ($d \sim \phi_v^{-s}$) with $s \sim 0.63$, where ϕ_v is the volume fraction of the nonaqueous components estimated from ϕ_s , using their densities. In the lamellar phase $s = 1.0$ and in the hexagonal phase it is 0.5. The intermediate value of s found here reflects a micellar morphology in between a cylinder and a bilayer, and it is consistent with the presence of mesh-like aggregates [12,38].

The CPC-SHN-water system shows both kinds of ordered mesh phases, and the transformation from the ordered mesh phase to L_α via L_α^D occurs with increasing temperature, concentration, or molar ratio. Both the Rh and the T mesh phases are also seen in the SDS-water system, but unlike in the present case they occur on either side of a bicontinuous cubic phase [39]. Therefore, these two phases have been identified as being of type I and type II, respectively [5]. In contrast, all the intermediate phases reported here are of type I and are made up of networks of rod-like micelles.

The CPC-SHN1-water system shows only the T and L_α^D mesh phases, and the Rh phase is absent here. Further, the intermediate phases in this system occur at relatively lower values of α compared to the CPC-SHN system. As mentioned earlier, counterions such as HN^- and HN1^- are known to be anchored at the micellar-water interface. However, their orientations at the micellar interface will be dissimilar, due to differences in the positions of the hydrophilic moieties. This is probably responsible for the observed differences in the phase behavior of the two mixtures.

In contrast to SHN and SHN1, the addition of DHN to CPC is not able to induce any kind of intermediate phase, and the phase behavior of this system is very similar to that of pure CPC. Although the DHN molecule can also be expected to preferentially sit at the micellar interface, its negligible effect on the phase behavior suggests that the electrostatic interaction between the surfactant head groups is the dominant factor in determining the curvature of the micelle-water interface. However, the stability of the mesh phases in the CPC-SHN and CPC-SHN1 systems cannot be attributed to the screening of the electrostatic repulsion between the head groups alone, since these phases are not usually seen with simple inorganic salts. Further, even some strongly binding counterions, such as salicylate and tosylate, do not induce these phases; for example, the phase diagram of the CPB-sodium salicylate and CPB-sodium tosylate systems at $\alpha = 1.0$ show only cylindrical worm-like micelles up to very high surfactant concentrations [40]. On the other hand, an alternative route between cylinders and bilayers, not involving any intermediate phases, has been observed in SDS- p -toluidine hydrochloride-water systems, with a

gradual change of the micellar morphology from cylindrical to disk-like [33]. Thus fine-tuning of many structural and interaction parameters seems to be necessary to stabilize the intermediate phases.

Theoretical considerations have shown the possibility of formation of type I mesh phases for values of the surfactant shape parameter $p (=v/al)$, where v is the volume of the hydrocarbon chain, l its optimal length, and a the optimal area of the head group) between 1/2 and 2/3 [5]. These studies also indicate that the tetragonal and hexagonal mesh structures, made up of genus 2 surfaces, are also the ones energetically most favored. However, the relative stability of these two phases is still poorly understood.

Intermediate phases have also been observed in diblock copolymers, which resemble surfactant systems in many ways because of their two chemically distinct parts [41]. Experimental and theoretical studies have shown that the bicontinuous gyroid phase is stable in these systems in between the hexagonal and the lamellar phase. On the other hand, mesh phases are not stable in these systems, although a metastable hexagonal perforated lamellar phase corresponding to the space group ($R\bar{3}m$), similar to the Rh mesh phase of surfactant-water systems, has been observed in some diblock copolymers.

The present system being multicomponent, detailed theoretical analysis is complicated by the likely existence of a coupling between local curvature and composition. Undoubtedly, this feature makes the phase behavior of the present systems very much richer than that of pure amphiphiles. We feel that computer simulations of systems such as the one studied here will lead to a better understanding of the stability of different intermediate phases. We hope that the present study will motivate future work in that direction.

V. CONCLUSIONS

The influence of two structurally isomeric organic salts, namely, SHN and SHN1, on the phase behavior of the cationic surfactant CPC has been investigated. Partial phase diagrams of the two systems have been constructed using POM and x-ray diffraction techniques. Intermediate phases are observed in both systems over a range of salt concentrations. All three known mesh phases are observed in the CPC-SHN-water system, whereas only the T and L_α^D phases are seen in the CPC-SHN1-water system. In addition, nematic phases made up of cylindrical and disk-like micelles are observed in one of the systems, for relatively low and high salt concentrations, respectively. These results show that the concentration of strongly binding counterions can be used as a control parameter to tune the spontaneous curvature of the micellar aggregates and stabilize different intermediate phases.

- [1] J. Israelachvili, *Intermolecular and Surface Forces*, 2nd ed. (Academic Press, London, 1991).
 [2] J. M. Seddon and R. H. Templer, in *Handbook of Biological Physics*, edited by R. Lipowsky and E. Sackmann (Elsevier, Amsterdam, 1995).

- [3] M. C. Holmes and M. S. Leaver, in *Bicontinuous Liquid Crystals*, edited by M. L. Lynch and P. T. Spicer, Surfactant Science Series, Vol. 127 (CRC Press, Boca Raton, FL, 2005), pp. 15–39.
 [4] V. Luzzati, in *Biological Membranes*, edited by D. Chapman (Academic Press, London, 1968).

- [5] S. T. Hyde, *Pure Appl. Chem.* **64**, 1617 (1992).
- [6] V. Luzzati, H. Mustachhi, A. E. Skoulios, and F. Husson, *Acta Crystallogr.* **13**, 660 (1960).
- [7] Y. Hendrikx and J. Charvolin, *J. Phys.* **42**, 1427 (1981).
- [8] G. Chidichimo, N. A. P. Vaz, Z. Yaniv, and J. W. Doane, *Phys. Rev. Lett.* **49**, 1950 (1982).
- [9] S. S. Funari, M. C. Holmes, and G. J. T. Tiddy, *J. Phys. Chem.* **96**, 11029 (1992).
- [10] S. S. Funari, M. C. Holmes, and G. J. T. Tiddy, *J. Phys. Chem.* **98**, 3015 (1994).
- [11] J. Burgoyne, M. C. Holmes, and G. J. T. Tiddy, *J. Phys. Chem.* **99**, 6054 (1995).
- [12] C. E. Fairhurst, M. C. Holmes, and M. S. Leaver, *Langmuir* **13**, 4964 (1997).
- [13] S. S. Funari and G. Rapp, *Proc. Natl. Acad. Sci. USA* **96**, 7756 (1999).
- [14] M. Leaver, A. Fogden, M. C. Holmes, and C. Fairhurst, *Langmuir* **17**, 35 (2001).
- [15] M. Imai, K. Nakaya, T. Kawakatsu, and H. Seto, *J. Chem. Phys.* **119**, 8103 (2003).
- [16] M. Imai, K. Sakai, M. Kikuchi, K. Nakaya, A. Saeki, and T. Teramoto, *J. Chem. Phys.* **122**, 214906 (2005).
- [17] M. Baciú, U. Olsson, M. S. Leaver, and M. C. Holmes, *J. Phys. Chem. B* **110**, 8184 (2006).
- [18] P. Kékicheff and B. Cabane, *J. Phys.* **48**, 1571 (1987).
- [19] P. Kékicheff and G. J. T. Tiddy, *J. Phys. Chem.* **93**, 2520 (1989).
- [20] M. S. Leaver and M. C. Holmes, *J. Phys. II France* **3**, 105 (1993).
- [21] S. Puntambekar, M. C. Holmes, and M. S. Leaver, *Liq. Cryst.* **27**, 743 (2000).
- [22] R. Zhou, M. C. Holmes, S. Puntambekar, M. S. Leaver, and R. McCabe, *Soft Matter* **8**, 5835 (2012).
- [23] B. F. B. Silva, E. F. Marques, and U. Olsson, *Soft Matter* **7**, 225 (2011).
- [24] R. Krishnaswamy, S. K. Ghosh, S. Lakshmanan, V. A. Raghunathan, and A. K. Sood, *Langmuir* **21**, 10439 (2005).
- [25] S. K. Ghosh, R. Ganapathy, R. Krishnaswamy, J. Bellare, V. A. Raghunathan, and A. K. Sood, *Langmuir* **23**, 3606 (2007).
- [26] S. K. Ghosh and V. A. Raghunathan, *Langmuir* **25**, 2622 (2009).
- [27] R. Oda, J. Narayanan, P. A. Hassan, C. Manohar, R. A. Salkar, F. Kern, and S. J. Candau, *Langmuir* **14**, 4364 (1998).
- [28] M. E. Cates and S. J. Candau, *J. Phys.: Condens. Matter* **2**, 6869 (1990).
- [29] T. Shikata, H. Hirata, and T. Kotaka, *Langmuir* **4**, 354 (1988).
- [30] A. Khatory, F. Lequeux, F. Kern, and S. J. Candau, *Langmuir* **9**, 1456 (1993).
- [31] V. Hartmann and R. Cressely, *J. Phys II France* **7**, 1087 (1997).
- [32] L. J. Yu and A. Saupe, *Phys. Rev. Lett.* **45**, 1000 (1980).
- [33] S. K. Ghosh, V. Rathee, R. Krishnaswamy, V. A. Raghunathan, and A. K. Sood, *Langmuir* **25**, 8497 (2009).
- [34] E. W. Kaler, K. L. Herrington, A. K. Murthy, and J. A. N. Zasadzinski, *J. Phys. Chem.* **96**, 6698 (1992).
- [35] M. T. Yacilla, K. L. Herrington, L. L. Brasher, and E. W. Kaler, *J. Phys. Chem.* **100**, 5874 (1996).
- [36] K. L. Herrington, E. W. Kaler, D. D. Millar, J. A. Zasadzinski, and S. Chiruvolu, *J. Phys. Chem.* **97**, 13792 (1993).
- [37] F. R. Husson and V. Luzzati, *J. Phys. Chem.* **68**, 3504 (1964).
- [38] S. T. Hyde, *J. Phys. Colloq.* **51**, C7 (1990).
- [39] P. Kékicheff and B. Cabane, *Acta Crystallogr.* **B44**, 395 (1988).
- [40] S. K. Ghosh, Ph.D. thesis, Jawaharlal University, New Delhi, 2007.
- [41] A. J. Meuler, M. A. Hillmyer, and F. S. Bates, *Macromolecules* **42**, 7221 (2009).